

Torpid Mixing of Markov Chains for the Six-vertex Model on \mathbb{Z}^2

Tianyu Liu

University of Wisconsin-Madison, Madison, WI, USA

tl@cs.wisc.edu

Abstract

In this paper, we study the mixing time of two widely used Markov chain algorithms for the six-vertex model, Glauber dynamics and the directed-loop algorithm, on the square lattice \mathbb{Z}^2 . We prove, for the first time that, on finite regions of the square lattice these Markov chains are torpidly mixing under parameter settings in the ferroelectric phase and the anti-ferroelectric phase.

2012 ACM Subject Classification Theory of computation → Design and analysis of algorithms, Theory of computation → Random walks and Markov chains

Keywords and phrases the six-vertex model, Eulerian orientations, square lattice, torpid mixing

Digital Object Identifier 10.4230/LIPIcs.APPROX-RANDOM.2018.52

Funding This work was supported by NSF CCF-1714275.

Acknowledgements The author thanks Professor Jin-Yi Cai for the valuable suggestions on the preliminary version of this paper.

1 Introduction

Introduced by Linus Pauling [23] in 1935 to describe the properties of ice, the *six-vertex model* or the *ice-type model* was originally studied in statistical mechanics as an abstraction of crystal lattices with hydrogen bonds. During the following decades, it has attracted enormous interest in many disciplines of science, and become one of the most fundamental models defined on the square lattice. In particular, the discovery of *integrability* of the six-vertex models with periodic boundary conditions was considered a milestone in statistical physics [16, 14, 15, 29, 10].

For computational expediency and modeling purposes, physicists almost entirely focused on planar lattice models. On the square lattice \mathbb{Z}^2 , every vertex is connected by an edge to four “nearest neighbors”. States of the six-vertex model on \mathbb{Z}^2 are orientations of the edges on the lattice satisfying the *ice-rule* — every vertex has two incoming edges and two outgoing edges, i.e., they are *Eulerian orientations*. The name of six-vertex model comes from the fact that there are six ways of arranging directions of the edges around a vertex (see Figure 1).

In general, each of the six local arrangements will have a weight, denoted by w_1, \dots, w_6 , using the ordering of Figure 1. The total weight of a state is the product of all vertex weights in the state. If there is no ambient electric field, by physical considerations, then the total weight of a state should remain unchanged when flipping all arrows [3]. Thus one may assume without loss of generality that $w_1 = w_2 = a, w_3 = w_4 = b, w_5 = w_6 = c$. This complementary invariance is known as *arrow reversal symmetry* or *zero field assumption*. In this paper, we assume $a, b, c > 0$, as is the case in *classical* physics. We study the six-vertex model restricted to a finite region of the square lattice with various boundary conditions customarily studied in statistical physics literature. On a finite subset $\Lambda \subset \mathbb{Z}^2$, denote the



© Tianyu Liu;

licensed under Creative Commons License CC-BY

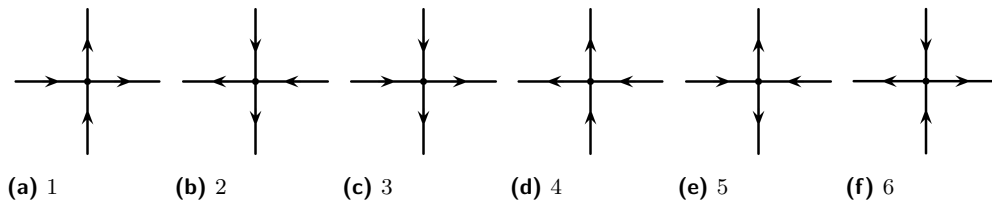
Approximation, Randomization, and Combinatorial Optimization. Algorithms and Techniques (APPROX/RANDOM 2018).

Editors: Eric Blais, Klaus Jansen, José D. P. Rolim, and David Steurer; Article No. 52; pp. 52:1–52:15



Leibniz International Proceedings in Informatics

Schloss Dagstuhl – Leibniz-Zentrum für Informatik, Dagstuhl Publishing, Germany



■ **Figure 1** Valid configurations of the six-vertex model.

set of valid configurations (i.e. Eulerian orientations) by Ω . The probability that the system is in a state $\tau \in \Omega$ is given by the Gibbs distribution

$$\mu(\tau) = \frac{1}{Z} (a^{n_1+n_2} b^{n_3+n_4} c^{n_5+n_6}),$$

where n_i is the number of vertices in type i ($1 \leq i \leq 6$) on Λ in the state τ , and the partition function Z is a normalizing constant which is the sum of the weights of all states.

In 1967, Elliot Lieb [16] famously showed that, for parameters $(a, b, c) = (1, 1, 1)$ on the square lattice graph, as the side N of the square approaches ∞ , the value of the “partition function per vertex” $W = Z^{1/N^2}$ approaches $(\frac{4}{3})^{3/2} \approx 1.5396007\dots$ (this is called Lieb’s square ice constant). This result is called an exact solution of the model, and is considered a triumph. After that, exact solutions for other parameter settings have been obtained in the limiting sense [14, 15, 29, 10]. Readers are referred to [7] for known results in the computational complexity of (both exactly and approximately) computing the partition function Z of the six-vertex model on *general* 4-regular graphs.

In statistical physics, *Markov chain Monte Carlo (MCMC)* is the most popular tool to numerically study the properties of the six-vertex model. A partial list includes [25, 31, 2, 9, 30, 1, 19]. In the literature, two Markov chain algorithms are mainly used. The first one is *Glauber dynamics*. It can be shown that there is a correspondence between Eulerian orientations of the *edges* and proper three-colorings of the *faces* on a rectangle region of the square lattice. (See Chapter 8 of [3] for a proof). Therefore, the Glauber dynamics for the three-coloring problem on square lattice regions (which changes a local color at each step) can be employed to sample Eulerian orientations. In fact, this simple Markov chain is used in numerical studies (e.g. in [9, 1, 19] for the density profile) of the six-vertex model under various boundary conditions. The second one is the *directed-loop algorithm*. Invented by Rahman and Stillinger [25] and widely adopted in the literature (e.g., [31, 2, 30]), the transitions of this algorithm are composed of creating, shifting, and merging of two “defects” on the edges. An interesting aspect is that this process depicts the *Bjerrum defects* happening in real ice [2]. More detailed descriptions of the two Markov chain algorithms can be found in Section 2.

With the heavy usage of MCMC in statistical mechanics for the six-vertex model, the efficiency of Markov chain algorithms was inevitably brought into focus by physicists. Many of them (e.g. [2, 30, 19]) reported that Glauber dynamics and the directed-loop algorithms of the six-vertex model experienced significant slowdown and are even “impractical” for simulation purposes when the parameter settings are in the *ordered phases* (see Figure 2a, in the regions FE & AFE). Despite the concern and numerical experience for the convergence rate of these algorithms, there is no previous provable result except for one point (that corresponds to the unweighted case) in the parameter space. This is in stark contrast to the popular studies on the mixing rate of Markov chains for the ferromagnetic Ising model [20, 21, 8, 17] and hardcore gas model on lattice regions [5, 26, 4].

Prior to [7], to our best knowledge, the only provable result in the complexity of approximate sampling and counting for the six-vertex model is at the single, *unweighted*, parameter setting $(a, b, c) = (1, 1, 1)$ where the partition function counts Eulerian orientations. In the unweighted case, all known results are positive. Mihail and Winkler's pioneering work [22] gave the first *fully polynomial randomized approximation scheme (FPRAS)* for the number of Eulerian orientations on a general graph (not necessarily 4-regular). Luby, Randall, and Sinclair showed that Glauber dynamics with extra moves is rapidly mixing on rectangular regions of the square lattice with fixed boundary conditions [18]. Randall and Tetali proved the rapid mixing of the Glauber dynamics (without extra moves) with fixed boundary conditions by a comparison technique applied to this Markov chain and the Luby-Randall-Sinclair chain [27]. Goldberg, Martin, and Paterson extended further the rapid mixing of Glauber dynamics to the free-boundary case [11]. The unweighted setting is the single green point depicted in the blue region of Figure 2b.

In [7], Cai, Liu, and Lu showed that under parameter settings (a, b, c) with $a^2 \leq b^2 + c^2$, $b^2 \leq a^2 + c^2$, and $c^2 \leq a^2 + b^2$ (the blue region in Figure 2b), the directed-loop algorithm mixes in polynomial time with regard to the size of input for any general 4-regular graph, resulting in an FPRAS for the partition function of the six-vertex model. Moreover, it is shown that in the ordered phases (FE & AFE in Figure 2a), the partition function on a general graph is not efficiently approximable unless NP=RP. Although the rapid mixing property for the directed-loop algorithm on general 4-regular graphs implies the same on the lattice region, the hardness result for general 4-regular graphs has no implications on the mixing rate of Markov chains for the six-vertex model on the square lattice in the ordered phases (FE & AFE).

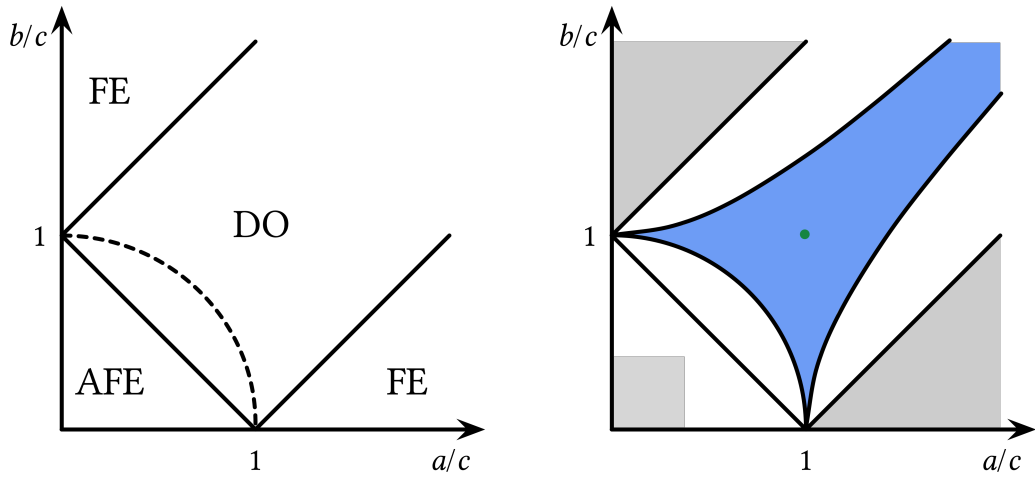
In this paper, we give the first provable negative results on mixing rates of the two Markov chains for the six-vertex model under parameter settings in the ferroelectric phases and the anti-ferroelectric phase. Our results conform to the phase transition phenomena in physics. Here we briefly describe the phenomenon of phase transition of the zero-field six-vertex model (see Baxter's book [3] for more details). On the square lattice in the thermodynamic limit: (1) When $a > b + c$ (FE: ferroelectric phase) any finite region *tends to* be frozen into one of the two configurations where either all arrows point up or to the right (Figure 1-1), or all point down or to the left (Figure 1-2). (2) Symmetrically when $b > a + c$ (also FE) all arrows point down or to the right (Figure 1-3), or all point up or to the left (Figure 1-4). (3) When $c > a + b$ (AFE: anti-ferroelectric phase) configurations in Figure 1-5 and Figure 1-6 alternate. (4) When $c < a + b$, $b < a + c$, and $a < b + c$, the system is disordered (DO: disordered phase) in the sense that all correlations decay to zero with increasing distance; in particular on the dashed curve $c^2 = a^2 + b^2$ the model can be solved by Pfaffians exactly [10], and the correlations decay inverse polynomially, rather than exponentially, in distance. See Figure 2a.

Let Λ be a square region on the square lattice. We show the following two theorems.

► **Theorem 1.1** (Ferroelectric phase). *The directed-loop algorithm for the six-vertex model under parameter settings (a, b, c) with $a > b + c$ or $b > a + c$ (i.e. the whole FE) mixes torpidly on Λ with periodic boundary conditions.*

► **Remark.** We note that for *periodic boundary conditions* Glauber dynamics is *not* irreducible, so we do not consider that.

► **Theorem 1.2** (Anti-ferroelectric phase). *Both Glauber dynamics and the directed-loop algorithm for the six-vertex model under parameter settings (a, b, c) with $c \geq 2.639 \max(a, b)$ (in AFE) mix torpidly on Λ with free boundary conditions and periodic boundary conditions.*



(a) Phase diagram of the six-vertex model.

(b) Mixing time of Markov chains for the six-vertex model on \mathbb{Z}^2 .

Figure 2

Parameter settings covered by the above two theorems are depicted as the grey region in Figure 2b. Given that the *F model* in statistical mechanics is a special case of the six-vertex model when $a = b = 1$ [14], Theorem 1.2 holds for the *F model* with $c \geq 2.639$.

Our proofs build on the equivalence between small conductance and torpid mixing by Jerrum and Sinclair [28]. When arguing Markov chains for the six-vertex model in the anti-ferroelectric phase have small conductance, we switch our view between finite regions of the square lattice and their *medial graphs*. This transposition allows us to adopt a *Peierls argument* which has been used in statistical physics to prove the existence of phase transitions (e.g., [24, 6]), and in theoretical computer science to prove the torpid mixing of Markov chains (e.g., [26, 4]).

In the proof of Theorem 1.2, we introduce a version of the *fault line argument* for the six-vertex model. Fault line arguments are introduced by Dana Randall [26] for the lattice hardcore gas and latter adapted in [13] for the lattice ferromagnetic Ising, which proves torpid mixing of Markov chains via topological obstructions. The constant 2.639 comes from an upper bound for the connective constant for the square lattice self-avoiding walks [12].

2 Preliminaries

2.1 Markov chains

2.1.1 Glauber dynamics

Denote by Λ_n a square lattice region where there are n vertices of degree 4 on each row and each column. Λ_n is in *periodic boundary condition* if it forms a two-dimensional torus; the *free boundary condition* can be formulated in the following way: there are $n + 2$ vertices on each row and each column, where the “boundary vertices” are of degree 1 and don’t need to satisfy the ice-rule (and don’t take weights) in a valid six-vertex configuration. For convenience, we assume there are “virtual edges” connecting every two boundary vertices with unit distance on \mathbb{Z}^2 . A virtual edge does not have orientations, serving only the purpose that every unit square inside the $(n + 1) \times (n + 1)$ region is closed.

Let Ω be the set of all valid configurations of the six-vertex model (Eulerian orientations) on Λ_n . The Glauber-dynamics Markov chain, which we will denote by \mathcal{M}_G , has state space Ω . To move from one configuration to another, this chain selects a unit square (a *face*) s on Λ_n (together with the virtual edges) uniformly at random. If all the non-virtual edges along the unit square s are oriented consistently (clockwise or counter-clockwise), the chain picks a direction d (clockwise or counter-clockwise) and reorients the non-virtual edges along s according to the Gibbs measure.

One can easily check that such transitions take valid configurations to valid configurations. Actually, this Markov chain is equivalent to that in [11] for sampling three-colorings on the faces of Λ_n . The ergodicity of that chain translates straightforwardly to the ergodicity of \mathcal{M}_G (with free boundary conditions) thanks to the equivalence between Eulerian orientations and three-colorings on \mathbb{Z}^2 . Besides, the heat-bath move indicates that the stationary distribution of \mathcal{M}_G is the Gibbs distribution for the six-vertex model.

2.1.2 Directed-loop algorithm

The directed-loop algorithm Markov chain, denoted by \mathcal{M}_D , is formally defined in [7] for general 4-regular graphs, so here we only describe \mathcal{M}_D at a high level.

The state space of \mathcal{M}_D is not only Ω , the “perfect” Eulerian orientations, but also the set of all “near-perfect” Eulerian orientations, denoted by Ω' . For example, in Figure 3 the state τ_{ur} is in Ω and all other five states are in Ω' . We think of each edge in Λ_n as the two half-edges cut in the middle, and each of the half edge can be oriented independently. We say an orientation of all the half-edges is *perfect* (in Ω) if every pair of half-edges is oriented consistently and the ice-rule is satisfied at every vertex (except for boundary vertices under free boundary conditions); an orientation is *near-perfect* (in Ω') if there are exactly two pairs of half-edges p_1 and p_2 not oriented consistently and the ice-rule is satisfied at every vertex (except for boundary vertices under free boundary conditions), with the restriction that if two half-edges in p_1 are oriented toward each other then in p_2 the two half-edges must be oriented against each other and vice versa.

The transitions in \mathcal{M}_D are Metropolis moves among “neighboring” states. An Ω state τ and an Ω' state τ' are neighboring if τ' can be transformed from τ by picking two half-edges e_1, e_2 incident to a vertex v with one pointing inwards v and the other pointing outwards v (or two half-edges e_1, e_2 on the boundary with one pointing towards the boundary and the other pointing against the boundary), and reverse the direction of e_1 and e_2 together. For instance, in Figure 3 $\{\tau_{ur}, \tau_{1b}\}$ and $\{\tau_{ur}, \tau_{1c}\}$ are two pairs of neighboring states. An Ω' state τ'_1 and another Ω' state τ'_2 are neighboring if τ'_2 can be transformed from τ'_1 by “shifting” one pair of conflicting half-edges one step away, while fixing the other pair of conflicting half-edges. For example, in Figure 3 τ_{1c} and τ_2 are neighboring to each other. \mathcal{M}_D can be proved to be ergodic and converges to the Gibbs measure on $\Omega \cup \Omega'$ with both free boundary conditions and periodic boundary conditions [7].

2.2 Mixing time

The *mixing time* t_{mix} measures the time required by a Markov chain to evolve to be close to its stationary distribution, in terms of *total variation distance*. (The definition of mixing time can be found in [13].) We say a Markov chain is torpid mixing if the mixing time is exponentially large in the input size. A common technique to bound the mixing time is via bounding conductance, defined by Jerrum and Sinclair [28].

Let π denote the stationary distribution of an *ergodic* and *time reversible* ($\pi(x)P(x, y) = \pi(y)P(y, x)$ for any $x, y \in \Omega$) Markov chain \mathcal{M} on a finite state space Ω , with transition probabilities $P(x, y)$, $x, y \in \Omega$. The *conductance* of \mathcal{M} is defined by

$$\Phi = \Phi(\mathcal{M}) = \min_{\substack{S \subset \Omega \\ 0 < \pi(S) \leq \frac{1}{2}}} \frac{Q(S, \bar{S})}{\pi(S)},$$

where $Q(S, \bar{S})$ denotes the sum of $Q(x, y) = \pi(x)P(x, y)$ over edges in the transition graph of \mathcal{M} with $x \in S$, and $y \in \bar{S} = \Omega \setminus S$.

In order to show a Markov chain mixes torpidly, we only need to prove that the conductance is (inverse) exponentially small due to the following bound [13]:

$$t_{\text{mix}} = t_{\text{mix}} \left(\frac{1}{4} \right) \geq \frac{1}{4\Phi}.$$

As is usually assumed, Markov chains studied in this paper are all *lazy* ($P(x, x) = \frac{1}{2}$ for any $x \in \Omega$) and transition probabilities ($P(x, y)$ for $x, y \in \Omega$) between neighboring states (where $P(x, y) > 0$) are at least inverse polynomially large. Therefore, armed with the above bound, we can prove the torpid mixing of a Markov chain if we can establish the following:

1. Partition the state space Ω into three subsets $\Omega_{\text{LEFT}} \cup \Omega_{\text{MIDDLE}} \cup \Omega_{\text{RIGHT}}$ as a disjoint union.
2. Show that for any state $\tau_l \in \Omega_{\text{LEFT}}$ and $\tau_r \in \Omega_{\text{RIGHT}}$, $P(\tau_l, \tau_r) = 0$. Under the assumption that the Markov chain is irreducible (i.e., the transition graph is strongly connected), this indicates that in order to go from states in Ω_{LEFT} to states in Ω_{RIGHT} , the Markov process has to go through the “middle states” Ω_{MIDDLE} .
3. Demonstrate that $\pi(\Omega_{\text{MIDDLE}})$ is exponentially small (compared with $\min(\pi(\Omega_{\text{LEFT}}), \pi(\Omega_{\text{RIGHT}}))$) in the input size. This means that starting from any state in Ω_{LEFT} , the probability of going through Ω_{MIDDLE} (and consequently to any state in Ω_{RIGHT} and reach stationarity) is exponentially small. Hence the conclusion of torpid mixing.

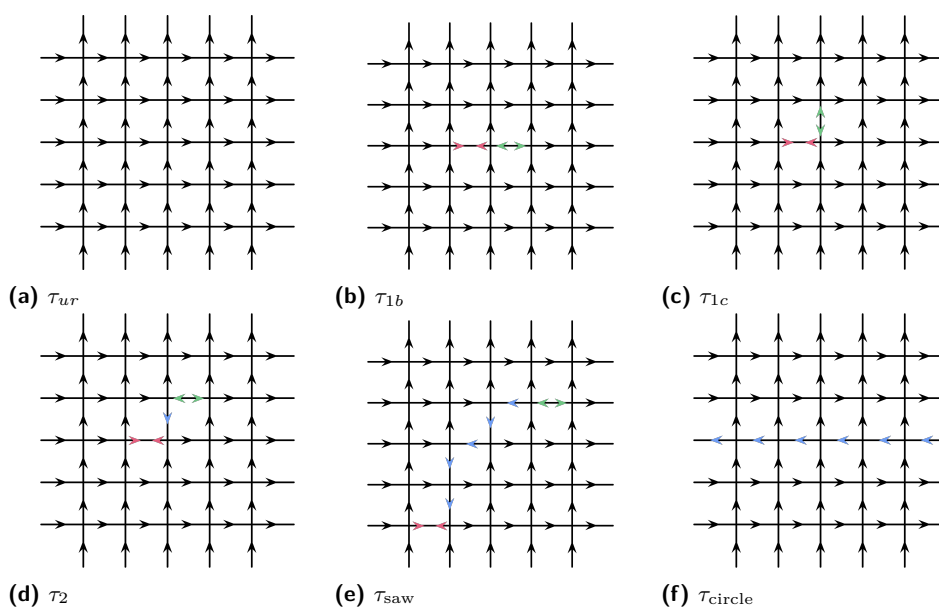
3 Ferroelectric phase

In this section we prove Theorem 1.1 that \mathcal{M}_D in the directed-loop algorithm for the six-vertex model in the ferroelectric phase is torpid mixing on Λ_n with periodic boundary conditions.

For any parameter setting (a, b, c) in the ferroelectric phase, either $a > b + c$ or $b > a + c$. By symmetry, without loss of generality, suppose $a > b + c$. This implies that vertex configurations as shown in Figure 1-1 and Figure 1-2 have higher weights than others. Under the periodic boundary condition, there is a state τ_{ur} in which every vertical edge points upwards and every horizontal edge points to the right (Figure 3a), i.e., every vertex on Λ_n is in local configuration shown in Figure 1-1. The total weight of τ_{ur} is a^{n^2} as there are n^2 vertices on Λ_n .

For \mathcal{M}_D , the three-way partition of the state space $\Omega \cup \Omega'$ is as follows. Denote by T_i the states that can be reached from τ_{ur} in at most i steps of transitions where i is a nonnegative integer. Write $\partial T_i = T_i \setminus T_{i-1}$ for $i \geq 1$. Let $\Omega_{\text{LEFT}} = T_{n-1}$, $\Omega_{\text{MIDDLE}} = \partial T_n$, and $\Omega_{\text{RIGHT}} = (\Omega \cup \Omega') \setminus (\Omega_{\text{LEFT}} \cup \Omega_{\text{MIDDLE}})$. It is obvious that $\Omega \cup \Omega' = \Omega_{\text{LEFT}} \cup \Omega_{\text{MIDDLE}} \cup \Omega_{\text{RIGHT}}$ is a partition of the state space. Clearly $\tau_{ur} \in \Omega_{\text{LEFT}}$, thus the total weight of Ω_{LEFT} is no less than a^{n^2} , the weight of τ_{ur} .

Before proving the total weight of Ω_{MIDDLE} is exponentially small compared with that of Ω_{LEFT} or Ω_{RIGHT} , let us look at what is in T_i with $0 \leq i \leq n$. T_0 is just $\{\tau_{ur}\}$. ∂T_1 consists



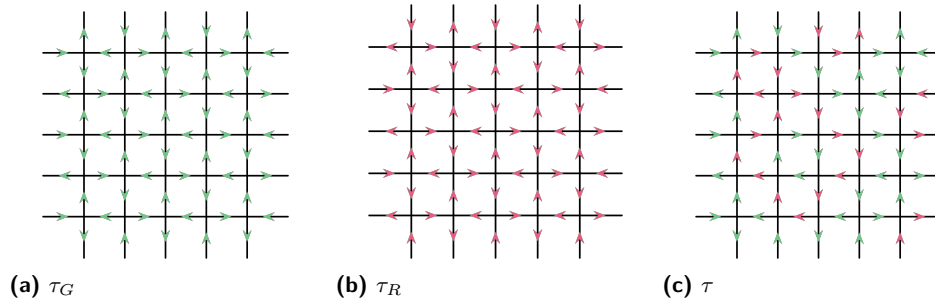
■ **Figure 3** Some states in the state space of \mathcal{M}_D .

of all the states evolved from τ_{ur} by picking a vertex v on Λ_n and two incident half-edges (one pointing towards v and the other away from v), and then reversing the orientations on these two edges. After such a transition, two pairs of conflicting half-edges are created, so $\partial T_1 \subseteq \Omega'$.

For example, the states shown in Figure 3b (state τ_{1b}) and Figure 3c (state τ_{1c}) are in ∂T_1 . The weight of τ_{1b} is $a^{n^2-1}b$ and that of τ_{1c} is $a^{n^2-1}c$. For every state in ∂T_1 obtained by transitions from τ_{ur} , there is exactly one vertex v^* on Λ_n no longer in the local configuration Figure 1-1. (Of course no vertex can be in state Figure 1-2.) Actually, depending on whether the two pairs of conflicting half-edges are: (1) both vertical, (2) both horizontal, or (3) one horizontal and the other vertical, the vertex v^* is in configuration shown in (1) Figure 1-3, (2) Figure 1-4, or (3) Figure 1-5/6, respectively. Therefore, every state in ∂T_1 has weight $a^{n^2-1}b$ in case (1) and case (2) or $a^{n^2-1}c$ in case (3).

Transitions from states in ∂T_1 to states in ∂T_2 are composed of “shifting” one of the two conflicting pairs of half-edges to a neighboring edge on Λ_n . For example, the state in Figure 3d is in ∂T_2 . This process will result in exactly two vertices on Λ_n not in local configuration Figure 1-1 (nor in Figure 1-2). As a consequence, the weight of any state in ∂T_2 is among $a^{n^2-2}b^2$, $a^{n^2-2}bc$, and $a^{n^2-2}c^2$. The state shown in Figure 3d has weight $a^{n^2-2}c^2$.

This line of argument can be extended for ∂T_i for $1 \leq i \leq n$, in any state of which there are exactly i vertices on Λ_n not in local configuration Figure 1-1 (nor in Figure 1-2). When two conflicting pairs of half-edges are created in ∂T_1 , one of them is above or to the right of another (or both). Denote the former by p_{ur} (the green pair in Figure 3) and the latter by p_{dl} (the red pair in Figure 3). Observe that as the Markov chain evolves, by a single step, from a state in ∂T_i to another in ∂T_{i+1} (where $1 \leq i \leq n-1$), either p_{ur} is “pushed” up or to the right, or p_{dl} down or to the left. For example, from Figure 3c to Figure 3d, p_{ur} is pushed to the right. By induction, p_{ur} is always above or to the right of p_{dl} (when $i < n$). A direct consequence is that there can be no state containing a closed circuit formed by the reversed edges (with regard to τ_{ur}) in ∂T_i until $i = n$. Therefore, the edges reversed in any state in ∂T_i ($1 \leq i \leq n$) can be seen as either a *self-avoiding walk* between the middle points of the



■ **Figure 4** Some states in the state space of \mathcal{M}_G .

two pairs of conflicting half-edges (e.g. Figure 3e) or a *self-avoiding circuit* (e.g. Figure 3f). In fact, when the reversed edges form a circuit, the circuit must “go straightforward” at each step. This circuit is a circle parallel or perpendicular to the torus equatorial plane. The weight of any state in ∂T_i is $a^{n^2-i} b^j c^k$ with $i = j + k$, where the values of j and k depend on how many “turnarounds” are there in the self-avoiding walk.

Therefore, the total weight of states in ∂T_n is at most $n^2 \cdot a^{n^2-n} (b+c)^n$, where n^2 is an upper bound on all the possible starting points for self-avoiding walks, and each monomial in $(b+c)^n$ is from a unique self-avoiding walk. Combining with the fact that total weight of Ω_{LEFT} is at least a^{n^2} (the weight of τ_{ur}) and is at most that of Ω_{RIGHT} (because there is a weight-preserving injective map from Ω_{LEFT} to Ω_{RIGHT} by reversing orientations of all the edges), we know that the conductance of \mathcal{M}_D is at most $\frac{n^2 \cdot a^{n^2-n} (b+c)^n}{a^{n^2}} = n^2 \left(\frac{b+c}{a}\right)^n$. This is exponentially small in n since $a > b+c$ are fixed constants in the ferroelectric phase.

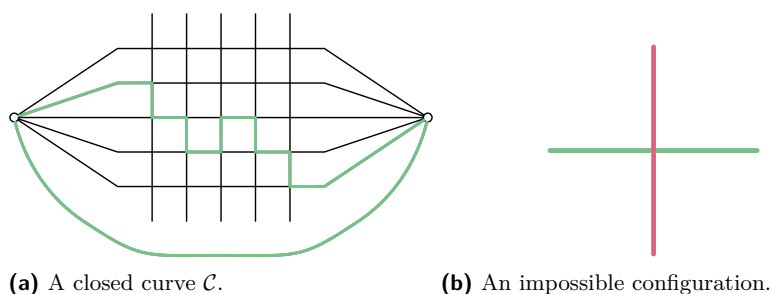
4 Anti-ferroelectric phase

In this section, we prove the following theorem which is part of Theorem 1.2. After proving Theorem 4.1, we state the ideas needed to extend it to Theorem 1.2, the full proof of which is omitted due to space limit.

As we did in the ferroelectric phase, the intuition behind our proof for the anti-ferroelectric phase is to find a partition $\Omega = \Omega_{\text{LEFT}} \cup \Omega_{\text{MIDDLE}} \cup \Omega_{\text{RIGHT}}$ of the state space of \mathcal{M}_G , i.e., all the Eulerian orientations on Λ_n . However, the strategy is different from that used in Section 3 — here the subset Ω_{MIDDLE} is determined in terms of a topological obstruction.

► **Theorem 4.1** (Anti-ferroelectric phase). *Glauber dynamics for the six-vertex model under parameter settings (a, b, c) with $c \geq 2.639 \max(a, b)$ mix torpidly on Λ_n with free boundary conditions.*

Observe that there are two states in Ω with maximum weights: τ_G (Figure 4a) and τ_R (Figure 4b) where every vertex is in local configuration Figure 1-5 or Figure 1-6, and thus has vertex weight c . Since τ_G and τ_R are total reversals of each other in edge orientations, for any edge in any state $\tau \in \Omega$, it is oriented either as in τ_G or as in τ_R . Let us call an edge to be *green* if it is oriented as is in τ_G and *red* otherwise. Observe that in order to satisfy the ice-rule (2-in-2-out), the number of green (and thus also two red) edges incident to any vertex (except for the boundary vertices) is always even (0, 2, or 4), and if there are two green (or red) edges they must be *rotationally adjacent* to each other. See Figure 4c for an example. Also note that the four edges along a unit square on \mathbb{Z}^2 are all red edges or all green edges if and only if they are oriented consistently, hence flippable by a single move of \mathcal{M}_G .



■ **Figure 5**

We say a simple path from a horizontal edge on the left boundary of Λ_n to a horizontal edge on the right boundary of Λ_n is a *horizontal green (or red) bridge* if the path consists of only green (or red, respectively) edges; a *vertical green (or red) bridge* is defined similarly. A state $\tau \in \Omega$ has a *green cross* if it has both a green horizontal bridge and a green vertical bridge; a *red cross* is defined similarly. Let $C_G \subset \Omega$ denote the states having a green cross and C_R the states having a red cross. In the following lemma, we prove that $C_G \cap C_R = \emptyset$.

► **Lemma 4.2.** *A green cross and a red cross cannot coexist.*

Proof. It suffices to show that a green horizontal bridge precludes a red vertical bridge. Consider a virtual point v_L sitting to the left of Λ_n connected by an edge to every (external) vertices of Λ_n on the left boundary, and another virtual point v_R connected by an edge to every vertex of Λ_n on the right boundary. Connect v_L and v_R by an edge below Λ_n .

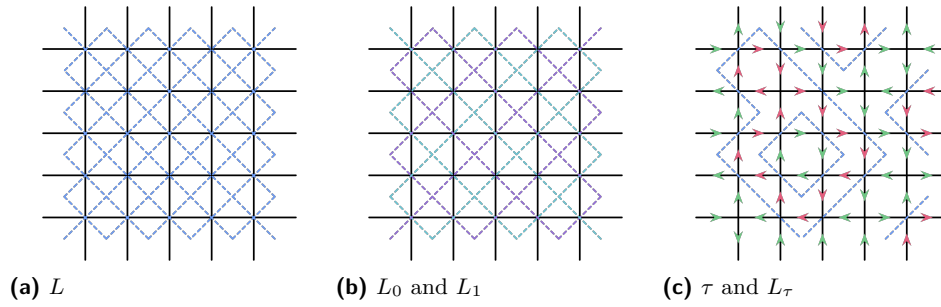
If there is a green horizontal bridge, then by definition there is a continuous closed curve \mathcal{C} formed by the bridge and some edges we added (Figure 5a). According to the *Jordan Curve Theorem*, \mathcal{C} separates the plane into two disjoint regions, the inside and the outside. Vertices of Λ_n that are on the bottom boundary are inside; vertices on the top boundary are outside. Therefore, in order to have a red vertical bridge, there must be a simple red path going across \mathcal{C} . That is to say, a red vertical bridge must cross the green horizontal bridge.

However, this is impossible. Clearly, being of different colors, a red bridge and a green bridge cannot share any edge. Since the local configuration shown in Figure 5b means that the four edges incident to a vertex (i, j) on Λ_n are all pointing inwards (when $i + j$ is even) or all pointing outwards (when $i + j$ is odd), it is not allowed in any valid states of six-vertex configurations. Similarly, the local configuration of a vertex surrounded by two red horizontal edges and two green vertical edges (a 90 degree rotation of Figure 5b) is also not allowed. ◀

Next we characterize the states in $\Omega \setminus (C_G \cup C_R)$. Define a shifted lattice¹ L to be $\mathbb{Z}^2 + (\frac{1}{2}, \frac{1}{2})$ where two points (a, b) and (c, d) in L are neighbors if $|a - c| = |b - d| = 1$ ($a, b, c,$ and d are all half integers), i.e., they are at the center of a square in \mathbb{Z}^2 and are connected by “diagonal” edges of length $\sqrt{2}$. An example of L and its relationship with \mathbb{Z}^2 is shown in Figure 6a. L is not connected — it is composed of two sub-lattices L_0 and L_1 (depicted with different colors in Figure 6b). Denote by L_n the restriction of L on the finite region inside Λ_n . Note that in graph theoretical terms, the square lattice Λ_n is planar and 4-regular, and thus can be seen as the *medial graph* of two planar graphs. In fact, they are L_0 and L_1 (restricted onto L_n).

From now on, we use Λ_n -vertices/edges as an abbreviation for vertices/edges in Λ_n ; and we use L_n -vertices/edges and other similar notations whenever it has a clear meaning in

¹ Strictly speaking, a lattice is a discrete subgroup of \mathbb{R}^n . A shifted copy of a lattice does not contain 0.



■ **Figure 6**

the context. For any state $\tau \in \Omega$, there is a subset L_τ of L_n -edges associated with τ . Each L_n -edge e “goes diagonally through” exactly one Λ_n -vertex, denoted by v_e . We say e is in L_τ if and only if the four Λ_n -edges incident to v_e are 2-green-2-red and e separates the two green edges from the two red edges (Remember that in this case edges in the same color must be rotationally adjacent to each other). See Figure 6c for an instance of a state τ and its associated L_τ . In the following we abuse the notation and use L_τ as its induced subgraph of L . This view was adopted by [6] for establishing the existence of the spontaneous staggered polarization in the anti-ferroelectric phase of the six-vertex model.

For any $\tau \in \Omega$ and L_τ , we make the following observations:

- There is always an even number of L_τ -edges meeting at any L_n -vertex, except for the L_n -vertices on the boundary. Because this number is equal to the number of times for the color change on the four Λ_n -edges surrounding the L_n -vertex, if we start from any one of the four Λ_n -edges and go rotationally over the four Λ_n -edges, which is even.
- For any Λ_n vertex, there can be at most one L_τ -edge going through which is either in L_0 or in L_1 .
- If $\bar{\tau} \in \Omega$ is the state by a total edge reversal of τ , then $L_{\bar{\tau}} = L_\tau$.

For a state $\tau \in \Omega$, we say τ has a *horizontal (or vertical) fault line* if there is a self-avoiding path in L_τ connecting a L_n -vertex on the left (top, respectively) boundary of L_n to a L_n -vertex on the right (bottom, respectively) boundary of L_n . See Figure 7c for an example where a state has both a horizontal fault line and a vertical fault line. Denote by C_{FL} the set of states containing a horizontal fault line or a vertical fault line. Since a fault line separates green edges from red edges, a vertical (horizontal) fault line precludes any horizontal (vertical, respectively) monochromatic bridge (the proof is basically the same as Lemma 4.2). This is to say, C_G , C_{FL} , and C_R are pairwise disjoint. Next we show the following lemma and its direct implication (Corollary 4.4).

► **Lemma 4.3.** *If in a state τ there is no monochromatic cross, then there is a fault line.*

Proof. If there is no monochromatic cross (i.e., a green cross or a red cross) in τ , we can assume that

there is no green horizontal bridge and there is no red horizontal bridge. (*)

- Suppose τ has a green horizontal bridge. There is no red vertical bridge since it cannot “cross” the green horizontal bridge; there is no green vertical bridge since there is no green cross. Therefore, this case is symmetric to (*), switching horizontal for vertical.
- Suppose τ has a red horizontal bridge. This case is similar to the above case, and thus is also symmetric to (*).

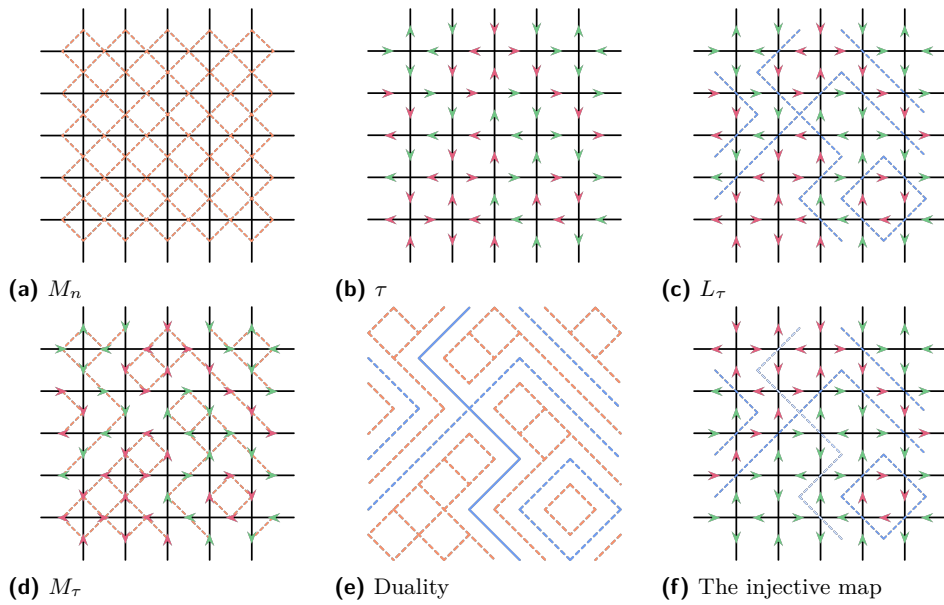


Figure 7

Next we show there is a vertical fault line if there is no monochromatic horizontal bridge. We introduce another graph M_n that is the *medial graph* of Λ_n where every vertex of M_n corresponds to an edge of Λ_n , i.e., two M_n -vertices are neighboring if the two corresponding Λ_n -edges are rotationally adjacent. Note that M_n is part of another shifted square lattice. An example of M_n and its relationship with \mathbb{Z}^2 is shown in Figure 7a. For any state $\tau \in \Omega$, there is a subset M_τ of M_n -edges associated with τ . An M_n -edge e is in M_τ if the two vertices that e is incident to (as Λ_n -edges) have the same color (both green or both red). See Figure 7d for an example.

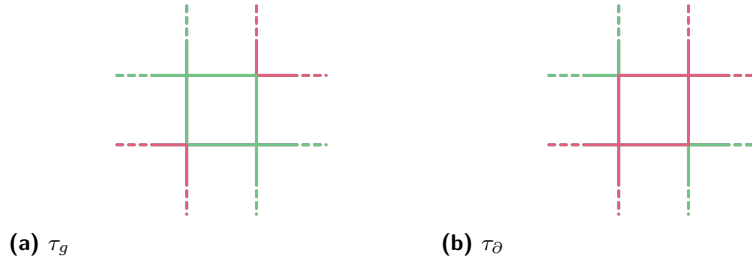
Observe that the correspondence between Λ_n -edges and M_n -vertices translates into the correspondence between simple monochromatic paths in Λ_n to simple connected paths in M_τ . In fact, the connected components in M_τ , capturing the notion of monochromatic regions of Λ_n -edges, and connected components in L_τ , capturing the notion of separation between regions of Λ_n -edges of different colors, are in a *dual* relationship.

This duality is depicted in Figure 7e and helps us find a fault line. Let V_M be the collection of M_n -vertices that can be reached from the left boundary of M_n by a simple path in M_τ . Since there is no monochromatic horizontal bridge, V_M does not contain any M_n -vertex on the right boundary. As a consequence, there is a *cutset* in M_n separating V_M from the right boundary. This cutset, composed of M_n -edges, corresponds to a vertical fault line. For instance, in Figure 7e the blue solid L_τ -path γ is a fault line defined by the above argument. ◀

► **Corollary 4.4.** $\Omega = C_G \cup C_{FL} \cup C_R$ is a partition of the state space.

Before moving on to prove Theorem 4.1, we introduce the notion of *almost fault lines*. A *horizontal (or vertical) almost fault line* is a self-avoiding L_n -path connecting a L_n -vertex on the left boundary of L_n to a L_n -vertex on the right boundary of L_n where all edges except for one are in L_τ . Denote by C_{AFL} the set of states containing an almost fault line. Let ∂C_G be the set of states outside C_G which are one-flip away from C_G in the state space of \mathcal{M}_G .

► **Lemma 4.5.** $\partial C_G \subset C_{FL} \cup C_{AFL}$.



■ **Figure 8** A step in \mathcal{M}_G .

Proof. If a state $\tau_\partial \in \partial C_G$ is not in C_{FL} (does not have a fault line), then by Corollary 4.4 $\tau_\partial \in C_R$ since by definition it is outside of C_G . Because τ_∂ is one move away from C_G , there exists a state $\tau_g \in C_G$ such that flipping four monochromatic edges along a unit square s on \mathbb{Z}^2 yields τ_∂ . We know that in τ_g there exists a green cross and no red cross; in τ_∂ there exists a red cross and no green cross. Then it must be true that the four edges along s are all green in τ_g and all red in τ_∂ . See Figure 8 for a pictorial illustration. Moreover, any green cross in τ_g must contain edges along s and so is any red cross in τ_∂ ; otherwise, a green horizontal (vertical) bridge in τ_g must go across a red vertical (or horizontal, respectively) bridge in τ_∂ at some other place on Λ_n , which is impossible.

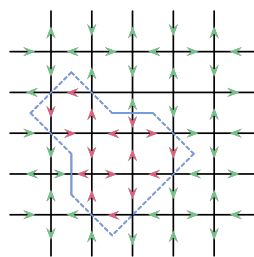
Therefore, there exists a simple green path Γ_G from some vertices on s to the top boundary of Λ_n and a simple red path Γ_R from some vertices on s to the top boundary of Λ_n . In the following, we prove that the above conditions suffice to show that there exists an L_τ -path from s to the top boundary of L_n . Similar conclusions can be made for the existence of L_τ -paths from s to the bottom boundary of L_n . By adding at most one L_n -edge, we can concatenate these paths to obtain a vertical almost fault line.

Γ_G and Γ_R cannot cross each other (Figure 5). Without loss of generality, suppose Γ_G is to the left of Γ_R . Then we use the medial lattice view M_{τ_∂} as in the proof of Lemma 4.3. Γ_G corresponds to a connected component m_G in M_{τ_∂} . Denote by V_G the set of M_n -vertices which can be reached by m_G in M_{τ_∂} , and let V'_G be V_G together with the set of M_n -vertices which are separated from the right boundary of M_n by V_G . Then there is a *cutset* in M_n separating V'_G from the right boundary. This cutset, composed of M_n -edges, corresponds to a dual L_τ -path from s to the top boundary of L_n . ◀

Now we are ready to show Theorem 4.1. Let $\Omega_{LEFT} = C_G$, $\Omega_{MIDDLE} = C_{FL} \cup (C_{AFL} \cap C_R)$, and $\Omega_{RIGHT} = C_R \setminus C_{AFL}$. Theorem 4.1 is a consequence of the following lemma which uses a *Peierls argument* to show that $\pi(C_{FL} \cup C_{AFL})$ is exponentially small.

► **Lemma 4.6.** $\pi(C_{FL} \cup C_{AFL}) \leq O(n) \left(\frac{2.639 \max(a,b)}{c} \right)^n$.

Proof. For a self-avoiding path γ in L_n connecting a vertex on the top boundary to a vertex on the bottom boundary, denote by F_γ the set of states in Ω that contain γ as vertical fault line or almost fault line. Reversing directions of all the edges to the left side of γ defines an injective mapping from F_γ to $\Omega \setminus F_\gamma$ that magnifies probability by a factor of at least $\frac{\min(a,b)}{c} \cdot \left(\frac{c}{\max(a,b)} \right)^{|\gamma|-1}$. This is because: if γ is a fault line in a state, every Λ_n -vertex sitting on γ would have four incident edges in the same color after the map, which increase its weight to c (from a or b); if γ is an almost fault line in a state, the above is true except that for one Λ_n -vertex, its weight decrease from c to a or b after the map, as orientations on half of the four monochromatic edges are reversed. This indicates that $\pi(F_\gamma) \leq \frac{c}{\min(a,b)} \cdot \left(\frac{\max(a,b)}{c} \right)^{|\gamma|-1}$.



■ **Figure 9** A state in \mathcal{M}_D .

See Figure 7f for an example. The same goes for horizontal (almost) fault lines.

Since every (almost) fault line is a self-avoiding walk on L , the number of fault lines of length l is upper bounded by $2n$ times the number of self-avoiding walks of that length starting at a vertex on the left or bottom boundary. The latter can be bounded by a well-studied estimate μ^l on the number of self-avoiding walks of length l on \mathbb{Z}^2 , where μ is called the *connective constant*. The best proved bound is $\mu \approx 2.638158 \dots$ [12]. Summing this over fault lines of length from n to n^2 completes the proof. ◀

We have proved the torpid mixing of Glauber dynamics for the six-vertex model on the lattice region Λ_n with free boundary conditions. Next we state the idea to extend the proof for the case when the Markov chain is \mathcal{M}_D and the case when the boundary of $\tilde{\Lambda}_n$ is periodic. Theorem 1.2 is a combination of Theorem 4.1 and the extensions.

To extend Theorem 4.1 to hold for the directed-loop algorithm \mathcal{M}_D whose state space is $\Omega \cup \Omega'$, we need to pay extra attention for the states in Ω' , the near-perfect Eulerian orientations. For a state $\tau' \in \Omega'$, there are two “defects” on the edges (Figure 9). Apart from the diagonal L_n -edges, there are two $(\mathbb{Z}^2 + (\frac{1}{2}, \frac{1}{2}))$ -edges separating green (half)-edges from red (half)-edges. The adaption we make is to put such $(\mathbb{Z}^2 + (\frac{1}{2}, \frac{1}{2}))$ -edges also into the set $L_{\tau'}$. Notice that a connected component in $L_{\tau'}$ could possibly lie on L_0 -edges as well as L_1 -edges. Everything we prove is still correct if we allow fault lines to have $(\mathbb{Z}^2 + (\frac{1}{2}, \frac{1}{2}))$ -edges. Due to the possible positions of such two defects, the weight of $C_{\text{FL}} \cup C_{\text{AFL}}$ only increases by a polynomial factor in n , hence not affecting the fact of torpid mixing.

To extend Theorem 4.1 to hold for $\tilde{\Lambda}_n$ with periodic boundary condition (i.e., a 2-dimensional torus), we make the following modification. When n is even, there still are two states with maximum weights c^{n^2} (similar to τ_G and τ_R in Figure 4). Again, for any state τ , $\tilde{\Lambda}_n$ -edges can be classified as green or red, and its associated L_τ separates $\tilde{\Lambda}_n$ -edges of different colors. For the 2-dimensional torus T^2 , the homology group $H_1(T^2) \cong \mathbb{Z} \times \mathbb{Z}$. We say a state τ has a *green (or red) cross* if there are two *non-contractable* cycles of green (or red, respectively) edges of *homology classes* (a_1, b_1) and (a_2, b_2) with $\det \begin{bmatrix} a_1 & a_2 \\ b_1 & b_2 \end{bmatrix} \neq 0$; τ has a *pair of fault lines* if there is a pair of non-contractable cycles of L_τ -edges. (By parity, if there is one L_τ -cycle there must be two.) Then the proofs in this section can be naturally adapted for the torus case, and the torpid mixing result follows.

References

- 1 David Allison and Nicolai Reshetikhin. Numerical study of the 6-vertex model with domain wall boundary conditions. *Annales de l'Institut Fourier*, 55(6):1847–1869, 2005. URL: <http://eudml.org/doc/116236>.
- 2 G. T. Barkema and M. E. J. Newman. Monte Carlo simulation of ice models. *Phys. Rev. E*, 57:1155–1166, Jan 1998. doi:10.1103/PhysRevE.57.1155.

- 3 R. J. Baxter. *Exactly Solved Models in Statistical Mechanics*. Academic Press, 1982. doi:10.1007/978-3-642-73193-8_19.
- 4 Antonio Blanca, David Galvin, Dana Randall, and Prasad Tetali. Phase coexistence and slow mixing for the hard-core model on \mathbb{Z}^2 . In *Approximation, Randomization, and Combinatorial Optimization. Algorithms and Techniques (APPROX/RANDOM)*, pages 379–394, 2013. doi:10.1007/978-3-642-40328-6_27.
- 5 Christian Borgs, Jennifer T. Chayes, Jeong Han Kim, Alan Frieze, Prasad Tetali, Eric Vigoda, and Van Ha Vu. Torpid mixing of some Monte Carlo Markov chain algorithms in statistical physics. In *Proceedings of the 40th Annual Symposium on Foundations of Computer Science (FOCS)*, pages 218–229, 1999. URL: <http://dl.acm.org/citation.cfm?id=795665.796518>.
- 6 H. J. Brascamp, H. Kunz, and F. Y. Wu. Some rigorous results for the vertex model in statistical mechanics. *Journal of Mathematical Physics*, 14(12):1927–1932, 1973. doi:10.1063/1.1666271.
- 7 Jin-Yi Cai, Tianyu Liu, and Pinyan Lu. Approximability of the six-vertex model. *CoRR*, abs/1712.05880, 2017. arXiv:1712.05880.
- 8 F. Cesi, G. Guadagni, F. Martinelli, and R. H. Schonmann. On the two-dimensional stochastic Ising model in the phase coexistence region near the critical point. *Journal of Statistical Physics*, 85(1):55–102, Oct 1996. doi:10.1007/BF02175556.
- 9 K. Eloranta. Diamond Ice. *Journal of Statistical Physics*, 96:1091–1109, 1999. doi:10.1023/A:1004644418182.
- 10 Chungpeng Fan and F. Y. Wu. General lattice model of phase transitions. *Phys. Rev. B*, 2:723–733, Aug 1970. doi:10.1103/PhysRevB.2.723.
- 11 Leslie Ann Goldberg, Russell Martin, and Mike Paterson. Random sampling of 3-colorings in \mathbb{Z}^2 . *Random Structures & Algorithms*, 24(3):279–302, 2004. doi:10.1002/rsa.20002.
- 12 A.J. Guttmann and A.R. Conway. Square lattice self-avoiding walks and polygons. *Annals of Combinatorics*, 5(3):319–345, Dec 2001. doi:10.1007/PL00013842.
- 13 David A. Levin, Yuval Peres, and Elizabeth L. Wilmer. *Markov chains and mixing times*. American Mathematical Society, 2006.
- 14 Elliott H. Lieb. Exact solution of the F model of an antiferroelectric. *Phys. Rev. Lett.*, 18:1046–1048, Jun 1967. doi:10.1103/PhysRevLett.18.1046.
- 15 Elliott H. Lieb. Exact solution of the two-dimensional Slater KDP model of a ferroelectric. *Phys. Rev. Lett.*, 19:108–110, Jul 1967. doi:10.1103/PhysRevLett.19.108.
- 16 Elliott H. Lieb. Residual entropy of square ice. *Phys. Rev.*, 162:162–172, Oct 1967. doi:10.1103/PhysRev.162.162.
- 17 Eyal Lubetzky and Allan Sly. Critical Ising on the square lattice mixes in polynomial time. *Communications in Mathematical Physics*, 313(3):815–836, Aug 2012. doi:10.1007/s00220-012-1460-9.
- 18 Michael Luby, Dana Randall, and Alistair Sinclair. Markov chain algorithms for planar lattice structures. *SIAM Journal on Computing*, 31(1):167–192, 2001. doi:10.1137/S0097539799360355.
- 19 I Lyberg, V Korepin, and J Viti. The density profile of the six vertex model with domain wall boundary conditions. *Journal of Statistical Mechanics: Theory and Experiment*, 2017(5):053103, 2017. URL: <http://stacks.iop.org/1742-5468/2017/i=5/a=053103>.
- 20 F. Martinelli and E. Olivieri. Approach to equilibrium of Glauber dynamics in the one phase region. I. the attractive case. *Communications in Mathematical Physics*, 161(3):447–486, Apr 1994. doi:10.1007/BF02101929.
- 21 F. Martinelli and E. Olivieri. Approach to equilibrium of Glauber dynamics in the one phase region. II. the general case. *Communications in Mathematical Physics*, 161(3):487–514, Apr 1994. doi:10.1007/BF02101930.

- 22 M. Mihail and P. Winkler. On the number of Eulerian orientations of a graph. *Algorithmica*, 16(4):402–414, Oct 1996. doi:10.1007/BF01940872.
- 23 Linus Pauling. The structure and entropy of ice and of other crystals with some randomness of atomic arrangement. *Journal of the American Chemical Society*, 57(12):2680–2684, 1935. doi:10.1021/ja01315a102.
- 24 R. Peierls. Statistical theory of adsorption with interaction between the adsorbed atoms. *Mathematical Proceedings of the Cambridge Philosophical Society*, 32(3):471–476, 1936. doi:10.1017/S0305004100019162.
- 25 Aneesur Rahman and Frank H. Stillinger. Proton distribution in ice and the Kirkwood correlation factor. *The Journal of Chemical Physics*, 57(9):4009–4017, 1972. doi:10.1063/1.1678874.
- 26 Dana Randall. Slow mixing of Glauber dynamics via topological obstructions. In *Proceedings of the Seventeenth Annual ACM-SIAM Symposium on Discrete Algorithm (SODA)*, pages 870–879, 2006. URL: <http://dl.acm.org/citation.cfm?id=1109557.1109653>.
- 27 Dana Randall and Prasad Tetali. Analyzing Glauber dynamics by comparison of Markov chains. *Journal of Mathematical Physics*, 41(3):1598–1615, 2000. doi:10.1063/1.533199.
- 28 Alistair Sinclair and Mark Jerrum. Approximate counting, uniform generation and rapidly mixing Markov chains. *Information and Computation*, 82(1):93–133, 1989. doi:10.1016/0890-5401(89)90067-9.
- 29 Bill Sutherland. Exact solution of a two-dimensional model for hydrogen-bonded crystals. *Phys. Rev. Lett.*, 19:103–104, Jul 1967. doi:10.1103/PhysRevLett.19.103.
- 30 Olav F. Syljuåsen and M. B. Zvonarev. Directed-loop Monte Carlo simulations of vertex models. *Phys. Rev. E*, 70:016118, Jul 2004. doi:10.1103/PhysRevE.70.016118.
- 31 A. Yanagawa and J.F. Nagle. Calculations of correlation functions for two-dimensional square ice. *Chemical Physics*, 43(3):329–339, 1979. doi:10.1016/0301-0104(79)85201-5.